

# First-principles study of electronic and diffusion properties of intrinsic defects in 4H-SiC

Cite as: J. Appl. Phys. **127**, 085702 (2020); doi: [10.1063/1.5140692](https://doi.org/10.1063/1.5140692)

Submitted: 2 December 2019 · Accepted: 7 February 2020 ·

Published Online: 24 February 2020



View Online



Export Citation



CrossMark

Xiaolan Yan, Pei Li, Lei Kang, Su-Huai Wei,<sup>a)</sup> and Bing Huang<sup>a)</sup>

## AFFILIATIONS

Beijing Computational Science Research Center, Beijing 100193, China

**Note:** This paper is part of the Special Topic on Defects in Semiconductors 2020.

<sup>a)</sup>**Authors to whom correspondence should be addressed:** [bing.huang@csrc.ac.cn](mailto:bing.huang@csrc.ac.cn) and [suhuaiwei@csrc.ac.cn](mailto:suhuaiwei@csrc.ac.cn)

## ABSTRACT

As a wide bandgap semiconductor, SiC holds great importance for high temperature and high power devices. It is known that the intrinsic defects play key roles in determining the overall electronic properties of semiconductors; however, a comprehensive understanding of the intrinsic defect properties in the prototype 4H-SiC is still lacking. In this study, we have systematically investigated the electronic properties and kinetic behaviors of intrinsic point defects and defect complexes in 4H-SiC using advanced hybrid functional calculations. Our results show that all the point defects in 4H-SiC have relatively high formation energies, i.e., low defect concentrations even at high growth temperatures. Interestingly, it is found that the migration barriers are very high for vacancies ( $>3$  eV) but relatively low for interstitial defects ( $\sim 1$  eV) in SiC. Meanwhile, the diffusion energy barriers of defects strongly depend on their charge states due to the charge-state-dependent local environments. Furthermore, we find that  $V_{Si}$  in SiC, a key defect for quantum spin manipulation, is unstable compared to the spin-unpolarized  $V_C-C_{Si}$  complex in terms of the total energy (under *p*-type conditions). Fortunately, the transformation barrier from  $V_{Si}$  to  $V_C-C_{Si}$  is as high as 4 eV, which indicates that  $V_{Si}$  could be stable at room (or not very high) temperature.

Published under license by AIP Publishing. <https://doi.org/10.1063/1.5140692>

## I. INTRODUCTION

Silicon carbide (SiC) is widely considered as an alternative to silicon (Si) in the high temperature and high-voltage power devices because of its unique physical properties, i.e., wide bandgap, high breakdown electric field strength, and high thermal conductivity.<sup>1–2</sup> The breakdown field strength of SiC is about ten times higher than that of Si, enabling the SiC devices to be much thinner with lower conduction and switching loss. Due to its high thermal conductivity, SiC has been widely used in high temperature and high power device applications.<sup>3–5</sup> Because of its wide bandgap and radiation hardness, the performance of SiC devices can maintain good stability even under strong irradiation environments.<sup>6–8</sup> In addition, it has been proposed that Si vacancy ( $V_{Si}$ ) can be used as a quantum bit because its spin states can be manipulated for quantum computing at room temperature.<sup>9–11</sup>

The understanding of the intrinsic defect properties in SiC, which play a critical role in determining its overall electric properties, is of great importance for the development of SiC-based electronic devices. Among its various allotropes, 4H-SiC is widely adopted in high-power devices, due to its high electron mobility

and availability of high-quality epitaxial wafers.<sup>1,4</sup> The major intrinsic defects that largely deteriorate the electronic properties of 4H-SiC are labeled as  $Z_{1/2}$ <sup>12</sup> and  $EH_{6/7}$ ,<sup>13</sup> which are generally found in epitaxial 4H-SiC.<sup>14–18</sup> The defect levels of  $Z_{1/2}$  and  $EH_{6/7}$  are located at 0.5–0.7 eV and 1.5–1.6 eV below the conduction band minimum (CBM), respectively, as detected by the deep-level transient spectroscopy (DLTS).<sup>19,20</sup> Since it is difficult to directly identify the defect types for  $Z_{1/2}$  and  $EH_{6/7}$  in the experiments, the extensive theoretical calculations have been carried out for this purpose, e.g., some calculations suggest that carbon vacancy defects are the main sources for the  $Z_{1/2}$  and  $EH_{6/7}$  levels.<sup>21–25</sup>

The intrinsic defects in 3C-SiC, including vacancies, antisites, and interstitials, have been studied using local-density approximation (LDA) calculations.<sup>26–28</sup> Meanwhile, several point defects, e.g., vacancies and divacancies, have also been investigated in 4H- and 6H-SiC.<sup>29,30</sup> However, it is well-known that LDA-level calculations could seriously underestimate the bandgap of semiconductors, which may make their calculated defect properties unreliable. Although the defect properties of vacancies in 3C- and 4H-SiC have also been investigated using Hyde–Scuseria–Ernzerhof (HSE)

hybrid functional<sup>31,32</sup> with corrected bandgap,<sup>21,33</sup> a systematic understanding of all the intrinsic defects in 4H-SiC, including their diffusion properties using HSE functional, is still lacking, which is the main purpose of our study.

In this study, the advanced HSE06 hybrid functional is adopted to calculate intrinsic defect properties in 4H-SiC. Our results show that all the point defects in intrinsic 4H-SiC have high formation energies, which correspond to the low defect concentrations at thermal equilibrium growth conditions. Meanwhile, we find that the vacancies have high migration barriers ( $\sim 3$  eV), whereas the interstitial defects have low energy barriers ( $\sim 1$  eV) in SiC. Interestingly, the diffusion barriers of defects could also strongly depend on their charge states, which is mainly due to the different local distortion around the defects at different charge states. Furthermore, we find that  $V_{Si}$  is unstable because it can convert to the  $V_C-C_{Si}$  complex with a lower total energy under *p*-type conditions. Fortunately, the transformation barrier from  $V_{Si}$  to  $V_C-C_{Si}$  is  $\sim 4$  eV, which indicates that  $V_{Si}$  could be stable at room (or not very high) temperature.

## II. METHODOLOGY

### A. Computational details

All the calculations were carried out using the Vienna Ab initio Simulation Package (VASP).<sup>34</sup> The exchange-correlation energy was treated both with the generalized gradient approximation (GGA) in the Perdew–Burke–Ernzerhof (PBE) form<sup>35</sup> and with the screened HSE06 hybrid density functional.<sup>31,32</sup> The plane-wave cutoff for the wavefunction expansion was set to 400 eV. Sufficiently, *k*-points were selected to make the total energies of calculated systems converged. During the structural relaxations, a conjugate-gradient algorithm was used until the force on each atom was lower than 0.01 eV Å<sup>-1</sup>, and the total energy was converged to  $1.0 \times 10^{-5}$  eV. The spin-polarized calculations were considered for all the defects in 4H-SiC. For the  $4 \times 4 \times 1$  supercell (128 atoms), a  $2 \times 2 \times 2$  Monkhorst-Pack *k*-point mesh for integrations over the Brillouin zone are used in the calculations. The calculated lattice parameters are  $a = 3.07$  Å,  $c = 10.05$  Å, and the calculated bandgap is 3.19 eV in the HSE06 calculation, in good agreement with available experimental results.<sup>1</sup>

The single defect levels are obtained by comparing the defect levels in defect cells and the VBM (valence band maximum) in the perfect cells according to aligned core levels of atoms furthest away from the defect center in defect cells to that of the perfect cells. The single-*k*-point calculations were performed to determine the defect levels. For the calculations of migration barrier, the CI-NEB methods, an effective method for finding the saddle points and minimum energy paths between initial and final states,<sup>36</sup> are adopted. The total energy and the force on each atom were converged to  $< 1.0 \times 10^{-5}$  eV and  $< 0.02$  eV Å<sup>-1</sup>, respectively. The number of images depends on the distance of the diffusion path between initial and final states, the distance between each image is not less than 0.8 Å.

### B. Formation energies of defects

The formation energy ( $E^f$ ) of a defect can be evaluated as<sup>37</sup>

$$E^f(\alpha, q) = \Delta E(\alpha, q) + \sum_i n_i \mu_i + q E_F + \Delta E_{align}(\alpha, q), \quad (1)$$

where  $\Delta E(\alpha, q) = E(\alpha, q) - E(host) + \sum_i n_i E_i + q E_V$ .  $E(host)$  is the total energy of the supercell without a defect, and  $E(\alpha, q)$  is the total energy of a supercell with a defect in a charge state  $q$ .  $q$  is the number of electrons transferred from the supercell to the reservoirs in forming the defect cell and  $n_i$  is the number of atoms removed from or added into the supercell,  $E_i$  is the total energy of C or Si at its ground state, and  $\mu_i$  is the chemical potential of atom  $i$  with respect to  $E_i$ . In this work, two limiting chemical potential conditions were considered, i.e., C-rich and Si-rich. Meanwhile,  $\mu_{Si}$  and  $\mu_C$  are limited by the formation energy of bulk SiC. That is, the maximum value of  $\mu_C$  (under C-rich condition) is given by bulk diamond (defined as zero), while the minimum value of  $\mu_C$  (under C-poor condition) is the formation energy of SiC.  $E_V$  and  $E_F$  are the energy of valence band maximum (VBM) and the Fermi level with respect to VBM, respectively.  $\Delta E_{align}(\alpha, q)$  is determined by aligning the core levels of atoms furthest away from the defect center in defect cells to that of the perfect cells.

We also examine the charge-state transition levels (CTLs), which are defined as

$$\varepsilon(q_1/q_2) = \frac{(E(\alpha, q_1) + \Delta E_{align}(\alpha, q_1)) - (E(\alpha, q_2) + \Delta E_{align}(\alpha, q_2))}{q_2 - q_1} - E_V. \quad (2)$$

### C. Concentrations of defects

Under thermodynamic equilibrium condition, the concentration of defects obeys the Boltzmann distribution that is related to their formation energies  $E^f$ <sup>38</sup>

$$C = N_{sites} g_q \exp(-E^f(\alpha, q)/k_B T). \quad (3)$$

Here,  $N_{sites}$  is the number of sites that defects can be incorporated per volume,  $k_B$  is Boltzmann's constant,  $T$  is the temperature, and  $g_q$  is the degeneracy factor that equals to the number of possible electron configurations for different charge states. With the constraint of charge neutrality condition,

$$p_0 + N_D^+ = n_0 + N_A^-, \quad (4)$$

where  $p_0$  and  $n_0$  are the concentrations of thermally excited holes and electrons,  $N_D^+$  and  $N_A^-$  are the total concentrations of positive and negative charge induced by defects, respectively. The defect concentrations  $c$  and the Fermi energy level  $E_F$  can be calculated self-consistently as a function of  $T$  and the growth chemical potentials  $\mu_i$ .

At a given temperature, the  $p_0$  and  $n_0$  in Eq. (4) are determined by

$$p_0 = N v e^{-(E_F - E_V)/k_B T} = N v e^{-E_F/k_B T}, \quad N_v = 2 \frac{(2\pi m_p^* k_B T)^{3/2}}{h^3}, \quad (5)$$

$$n_0 = N_C e^{-(E_C - E_F)/k_B T} = N_C e^{(E_F - E_g)/k_B T}, \quad N_C = 2 \frac{(2\pi m_n^* k_B T)^{3/2}}{h^3}, \quad (6)$$

where  $E_V$  and  $E_C$  are VBM and CBM energies, and  $E_V$  generally set to 0, while  $E_C = E_g$  ( $E_g$  is the bandgap).  $N_V$  and  $N_C$  are the effective density of states (DOS) of the valence band and the conduction band,  $m_p^*$  and  $m_n^*$  are the effective mass of hole and electron, respectively.

In practice, quenching is often used to improve the defect property, in which the 4H-SiC can be grown under various high temperatures but quenched to room temperature. Therefore, we also calculate the defect concentrations under growth temperature (GT), and then quenching it to room temperature, keeping the sum of the defect densities fixed and recalculating the density of the charged defects at room temperature (RT). In this situation, the equilibrium  $E_F$  and carrier densities are changed before and after quenching.

### III. RESULTS AND DISCUSSION

The 4H-SiC has two inequivalent sites for C and Si, i.e., cubic sites ( $k$ ) and hexagonal sites ( $h$ ), as shown in Fig. 1. Our test calculations indicate that the defect states have similar characters at these two different sites (the detailed defect structures are shown as Fig. S1 in the supplemental material). For an ideal C vacancy ( $V_C$ ) or Si vacancy ( $V_{Si}$ ) defect, the remaining four dangling bonds located at the surrounding Si (C) atom sites give rise to two single  $a_1$  states and a double-degenerated  $e$  states, which is induced by the local crystal field splitting of  $C_{3v}$  symmetry. After the structural relaxation, the local symmetry around a vacancy will be reduced from  $C_{3v}$  to  $C_{1h}$ , which leads to the  $a_1$  states appearing as  $a'$  states and the  $e$  states splitting to  $a'$  and  $a''$  states. Our calculations confirm that the ground state of a  $V_C$  defect prefers a low-spin configuration, while  $V_{Si}$  prefers a high-spin state, as shown in Fig. 2. This difference is mainly caused by the difference of exchange interactions of the delocalized  $3p$  electrons of Si around a  $V_C$  and localized  $2p$  electrons of C atom around a  $V_{Si}$ . The defect levels of  $V_C$ , derived from its nearest neighbor Si

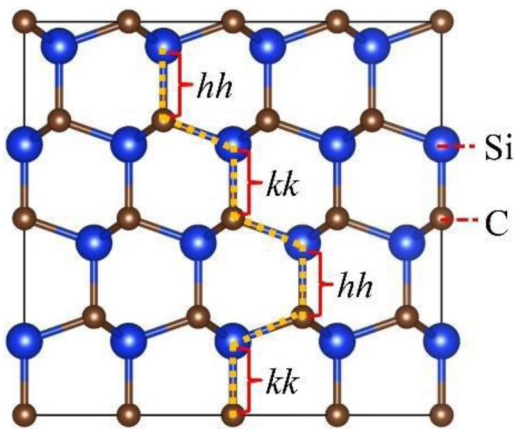


**FIG. 1.** Supercell structure of 4H-SiC used for defect calculations. Blue and brown balls indicate the Si and C atoms, respectively. There are two inequivalent lattice sites, named as  $h$ -site and  $k$ -site.

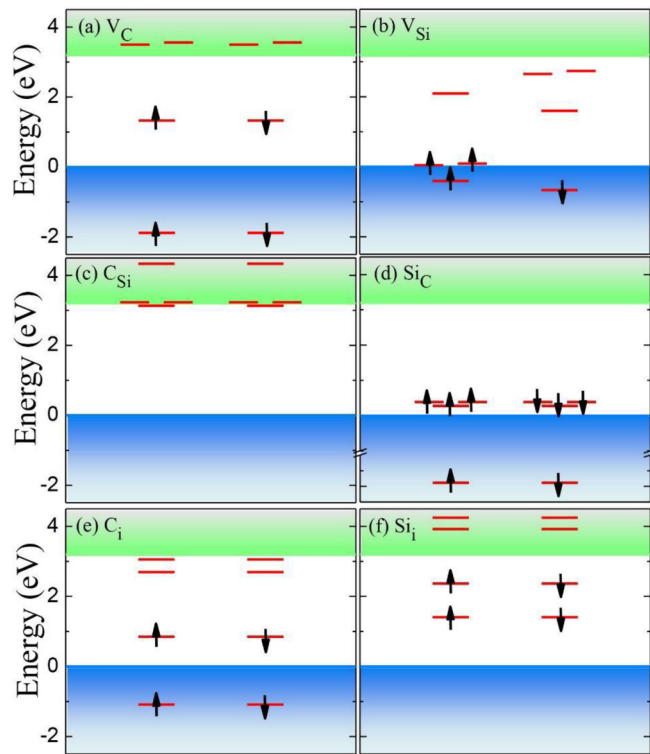


**FIG. 2.** Single-particle defect levels for the intrinsic defects at  $k$ -sites in 4H-SiC for (a)  $V_C$ , (b)  $V_{Si}$ , (c)  $C_{Si}$ , (d)  $Si_C$ , (e)  $C_i$ , and (f)  $Si_i$ . See text for the detailed explanations. Green and blue regions indicate the conduction band (CB) and the valence band (VB), respectively. The up and down arrows denote the occupied spin-states of electrons on the defect levels.

dangling bonds, lie closer to the CBM than that of  $V_{Si}$  [Figs. 2(a) and 2(b)]. For the cases of isovalent antisite defects, i.e., C on Si ( $C_{Si}$ ) and Si on C ( $Si_C$ ), their defect levels in the gap are fully empty [Fig. 2(c)] or occupied [Fig. 2(d)]. For the interstitial defects, i.e., C interstitials ( $C_i$ ), as shown in Fig. 2(e), one of the defect levels in the bandgap is occupied by two electrons while the other one is empty, which means that the  $C_i$  defect may further behave as  $-2$  or  $+2$  charge states when the  $E_F$  position is changed inside the bandgap. On the other hand, the empty  $Si_i$  defect levels are above the CBM, so they may only exhibit positive charge states.

We have also calculated the  $E^f$  and CTLS for these defects, as shown in Fig. 3. For each defect, there is a stable charge state with the lowest energy at each value of  $E_F$  (Fig. 3), i.e., once the  $E_F$  of the system is given, the stable charge states of all the defects can be obtained. The slope in Fig. 3 represents the charge state, and the vertices represent the CTLS between two different charge states. Interestingly, it is noted that the CTLS of defects at the  $h$ -site and  $k$ -site are different, even if they have a similar  $E^f$  at neutral states, except for the interstitial defects. Generally, the  $E^f$  of Si-related defects are higher than that of C-related defects. On the neutral charge state, the

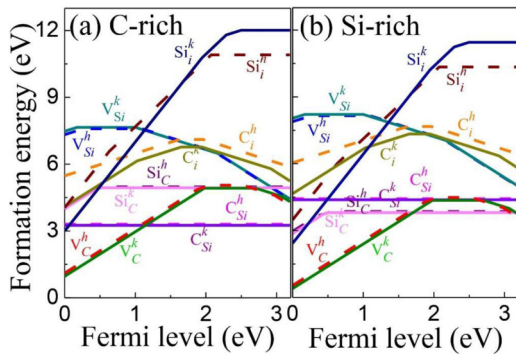


**FIG. 3.** Formation energies of intrinsic defects under (a) C-rich and (b) Si-rich chemical conditions. Solid and dashed lines indicate the defects located at *k*-sites and *h*-sites, respectively. Zero of Fermi level is set to the position of VBM.

antisite  $C_{Si}$  has a lower energy than  $Si_C$  defects because it is easier to substitute a small-size atom at a large-size atom site. Although the  $E^f$  of  $C_{Si}$  is lower in a large range of  $E_F$ , its defect level is resonated in the valence band. On the other hand, although the interstitial defects ( $Si_i$  and  $C_i$ ) have relatively high  $E^f$ , they still could be formed in a positive charge states under *p*-type growth conditions. The positively-charged and negatively-charged  $V_C$  become more favorable under *p*-type and *n*-type

growth conditions respectively, while negatively-charged  $V_{Si}$  is favorable under *n*-type growth conditions. Interestingly, the donor level of  $V_C$  is found to exhibit a negative-*U* behavior at the *k*-site. The 0/-1 CTLs of  $V_C$  is located around  $E_C - (0.5 - 0.7)$ , which is close to the position of  $Z_{1,2}$  observed in the experiments. Therefore, the  $V_C$  could be the most important defect that can downgrade the electronic properties of SiC during device applications.

After obtaining the  $E^f$  and CTLs of the intrinsic defects in 4H-SiC, we can estimate their defect concentrations at a given GT, while the working temperature is set to RT. SiC is generally grown at a high temperature, e.g., the common GT is 1850 K.<sup>1</sup> As can be seen in Fig. 4(a), the calculated  $E_F$  is located near the middle of the bandgap. This is because band-edge excitation dominates at this temperature, even though more intrinsic defects can be created when GT increases. When quenched to RT, the total concentration of all the defects is assumed fixed at that created at GT, but the concentrations of defects at different charge states can be redistributed. At RT, the thermally excited electrons and holes are significantly reduced. The amount of positively charged  $V_C$  induced electrons moves the  $E_F$  toward the CBM. The  $E^f$  of  $C_{Si}$  and  $Si_C$  are independent of the  $E_F$ . However, when  $E_F$  moves toward the CBM,  $V_C$  prefers to form negative charge states and the concentration of the negatively charged  $V_C$  increases. When the temperature quenched from 1850 K to 300 K, the defect concentration of  $V_C$  is about  $10^{12} \text{ cm}^{-3}$  under Si-rich condition, which is generally consistent with the experimental results.<sup>1</sup>

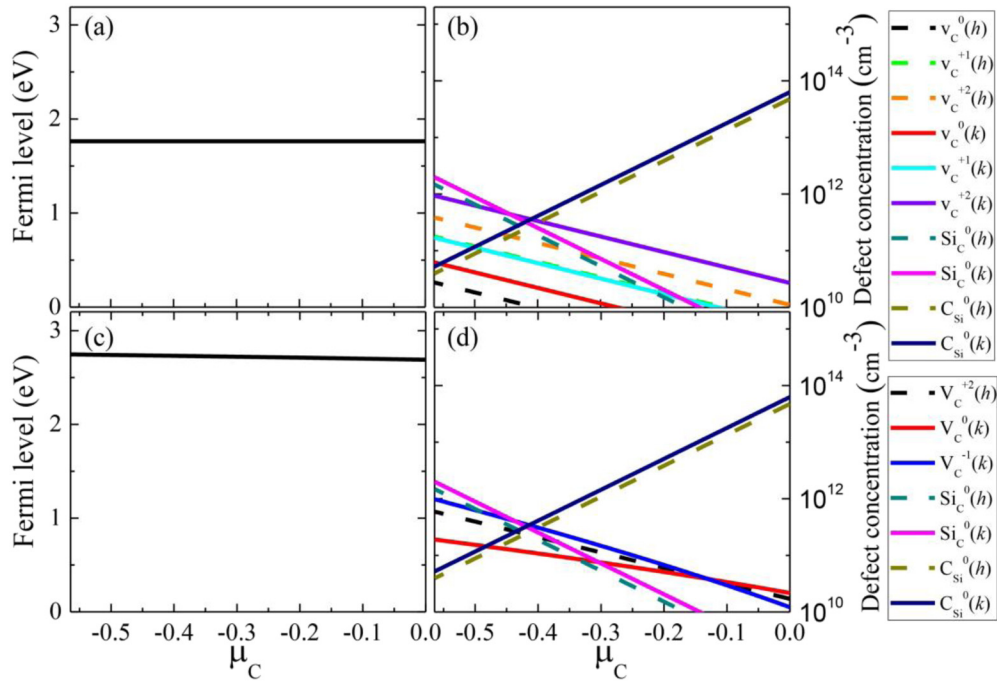


**FIG. 4.** Fermi energy  $E_F$  (left panel) and defect concentration (right panel) of intrinsic defects before: (a) and (b) and after: (c) and (d) quenching. Growth temperature is set to 1850 K, while working temperature is set to room temperature. Solid and dashed lines indicate the defects located at *k*-sites and *h*-sites, respectively.

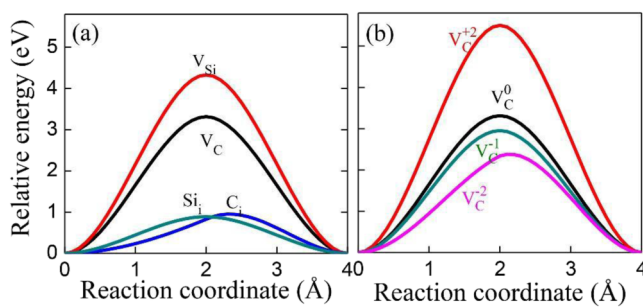


**FIG. 5.** (a) Diffusion barriers of various intrinsic defects in 4H-SiC; (b) diffusion barriers of  $V_C$  at different stable charge states. It is noted that the intermediate image structures for these defects along the reaction coordinates can be found in Fig. S2 in the [supplementary material](#).

Overall, the concentrations of all intrinsic defects in intrinsic 4H-SiC are relatively low.

In the experiments, the annealing process is necessary after the growth of 4H-SiC in order to reduce the native defect concentrations and improve its electronic properties.<sup>14,18</sup> During the annealing process, the defects can be reactivated and diffused. Therefore, it is also important to understand the diffusive properties of defects in 4H-SiC. In order to investigate the diffusion path of intrinsic defects, the CI-NEB methods<sup>36</sup> are used, and the results are shown in Fig. 5. It is found that the diffusion barriers of antisite defects are extremely high (~10 eV, not shown in Fig. 5), as the diffusion of C and Si simultaneously could give rise to the large local structural distortions (corresponding to high strain energies). For isolated vacancies, their diffusion barriers are also very large, i.e., 3.3 eV for  $V_C$  and 4.3 eV for  $V_{Si}$ . On the other hand, it is found that the interstitial defects have relatively low energy barriers, i.e., 0.95 eV for  $C_i$  and 0.88 eV for  $Si_i$ , which indicates that they could diffuse fast during the annealing process at high temperature. The intermediate image structures for these defects along the reaction coordinates can be found in Fig. S2 in the [supplementary material](#).

Interestingly, it is also found that the charge states of a defect can strongly affect its diffusion barrier. Taking  $V_C$  as a typical example, we have calculated the diffusion barriers of  $V_C$  at different possible charge states, as shown in Fig. 5(b). Interestingly, the calculated diffusion barriers of  $V_C$  gradually increase as its charge states change from negative to positive ones, which is accompanied by a large outward atomic relaxation effects around the defect sites. Therefore, the structural changes caused by the different electron occupations of  $V_C$  are the major reason for the charge-state-dependent diffusion barrier. Similarly, the migration barriers for  $V_{Si}$  and interstitials also exhibit charge-state-dependent behaviors, as shown in Fig. S3 in the [supplemental material](#).

Besides the single point defects, the defect complexes could also exist in 4H-SiC, e.g., antisite-vacancy pair ( $V_C-C_{Si}$ ) and divacancy ( $V_C-V_{Si}$ ) are two typical examples. In practice,  $V_C-C_{Si}$  may also be transformed from  $V_{Si}$ , as the  $E'$  of  $V_C-C_{Si}$  under the neutral state is ~0.6 eV lower than that of  $V_{Si}$ , as shown in Fig. 6(a). According to the charge state calculations,  $V_C-C_{Si}$  is more stable under *p*-type condition but  $V_{Si}$  is more stable under *n*-type condition. The ground-state of  $V_C-C_{Si}$  is spin unpolarized, which is different from that of single  $V_{Si}$ . Therefore, the transformation from high-energy  $V_{Si}$  to low-energy  $V_C-C_{Si}$  under *p*-type condition could fundamentally eliminate the NV-center-like function of  $V_{Si}$ . However, the calculated energy diffusion barrier between the  $V_C-C_{Si}$  and  $V_{Si}$  is ~4 eV as shown in Fig. 6(b), indicating that  $V_{Si}$  still maybe stable at room-temperature once it can be formed.

For a  $V_C-V_{Si}$  divacancy, there are four inequivalent structures. As shown in Fig. 7,  $V_C-V_{Si}$  always exhibits high-spin configurations independent of its different local structures. The defect levels of  $V_C-V_{Si}$  can be understood as a combination of individual  $V_C$  and  $V_{Si}$ . In the cases of *kk*- and *hh*-divacancy structures, the degenerated *e* states originated from  $V_C$  and  $V_{Si}$  can maintain. While for *kh*- and *hk*-divacancy, the *e* states will be split to *a'* and *a''* states. The  $E'$  of  $V_C-V_{Si}$  is around 8.2 eV, which is independent of the chemical potentials. As shown in Fig. 6(c), the calculated diffusion barrier of  $V_C-V_{Si}$  divacancy is as high as ~4.5 eV.

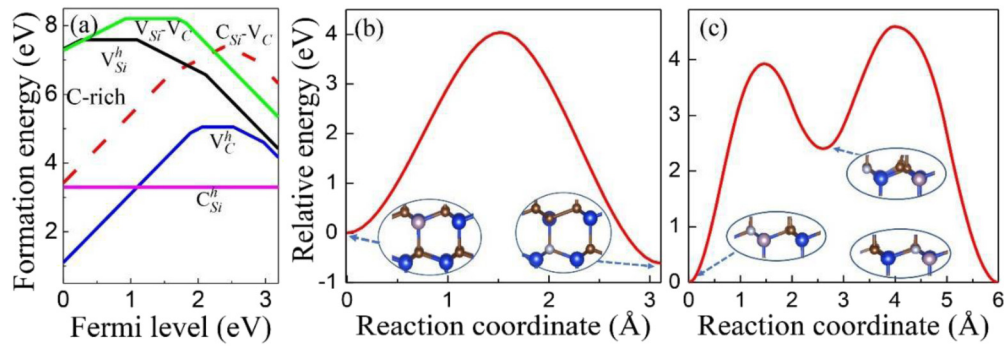


**FIG. 6** (a) Formation energies of  $V_C-C_{Si}$  and  $V_C-V_{Si}$  defect complexes compared with single point defects under C-rich condition; (b) calculated diffusion barrier between  $V_{Si}$  and  $V_C-C_{Si}$ ; and (c) calculated diffusion barrier for the  $V_C-V_{Si}$ . Pink and gray balls indicate the Si and C vacancies, respectively.

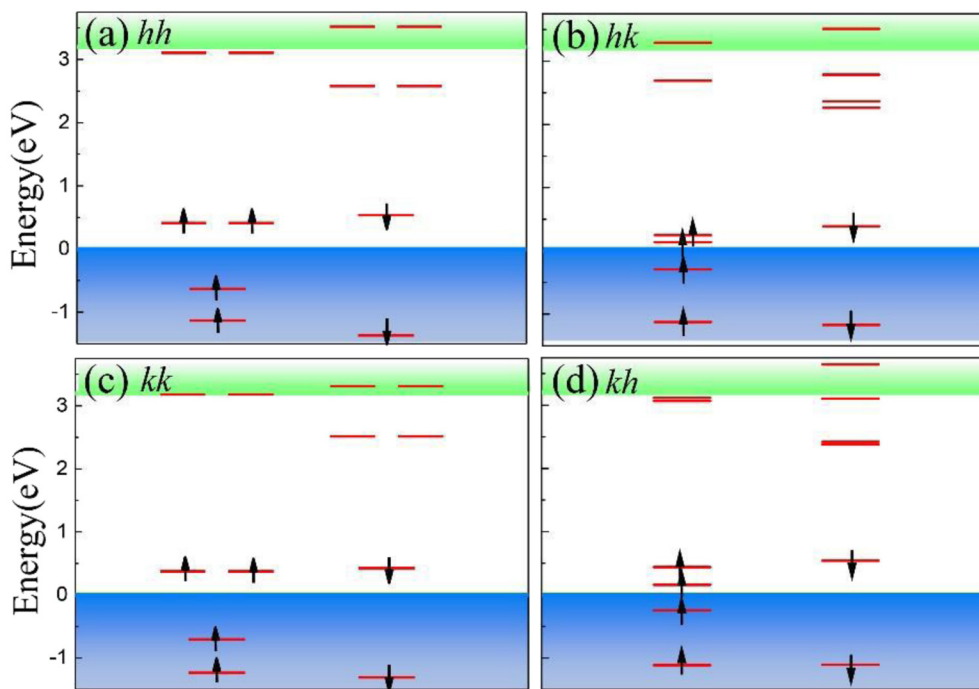


**FIG. 7** Single-particle defect levels of four different types of  $V_C$ - $V_{Si}$  in 4H-SiC: (a)  $hh$  combination; (b)  $hk$  combination; (c)  $kk$  combination; and (d)  $kh$  combination. Green and blue region indicate the conduction band (CB) and the valence band (VB) regions, respectively. The up and down arrows denote the occupied spin-states of electrons.

#### IV. CONCLUSION

The electronic and kinetic properties of intrinsic point defects and defect complexes in 4H-SiC have been systematically studied using advanced hybrid functional calculations. Among all the defects, antisite defects ( $C_{Si}$  and  $Si_C$ ) and  $V_C$  have relatively lower formation energies than other defects. Since the defect levels of antisite defects are electronically inactive, the dominant harmful defect in 4H-SiC could be a deep-level  $V_C$  defect. For the point defects, the diffusion barriers of interstitial defects are  $<1$  eV, while all the others are  $>3$  eV, indicating that the interstitial defects could diffuse very fast in the annealing process. Interestingly, the diffusion barriers of defects in 4H-SiC can strongly depend on their charge states. In addition, the  $V_C$ - $C_{Si}$  complex is found to have lower formation energy than that of  $V_{Si}$  at the neutral charge state, but the energy barrier for the formation of this defect complex is as high as 4 eV.

#### SUPPLEMENTARY MATERIAL

Local defect configurations of all the intrinsic defects, the image structures along the migration paths for  $V_C$ ,  $V_{Si}$ ,  $C_i$ , and  $Si_i$ , and diffusion energy barriers of  $V_{Si}$ ,  $C_i$ , and  $Si_i$  at stable charge states are shown in the [supplementary material](#).

#### ACKNOWLEDGMENTS

This work is supported by the Science Challenge Project under No. TZ2016003 and NSFC Program under Grant Nos.

51672023 and 11634003, and NSAF Program under Grant No. U1930402. All the computations were performed at Tianhe2-JK at CSRC.

#### REFERENCES

- <sup>1</sup>T. Kimoto and J. A. Cooper, *Fundamentals of Silicon Carbide Technology: Growth, Characterization, Devices and Applications* (Wiley-IEEE Press, 2014).
- <sup>2</sup>F. Wang and Z. Zhang, *CPSS Trans. Power Electron. Appl.* **1**, 13 (2016).
- <sup>3</sup>T. Kimoto, *Jpn. J. Appl. Phys.* **54**, 040103 (2015).
- <sup>4</sup>J. A. Cooper and A. Agarwal, *Proc. IEEE* **90**, 956 (2002).
- <sup>5</sup>F. Roccaforte, P. Fiorenza, G. Greco, R. Lo Nigro, F. Giannazzo, F. Iucolano, and M. Saggio, *Microelectron. Eng.* **187-188**, 66 (2018).
- <sup>6</sup>A. A. Lebedev and V. V. Kozlovskii, *Semiconductors* **48**, 1293 (2014).
- <sup>7</sup>M. Usman, A. Hallén, K. Gulbinas, and V. Grivickas, *Mater. Sci. Forum* **717-720**, 805 (2012).
- <sup>8</sup>V. V. Emtsev, A. M. Ivanov, V. V. Kozlovskii, A. A. Lebedev, G. A. Oganesyan, and N. B. Strokan, *Semiconductors* **44**, 678 (2010).
- <sup>9</sup>J. R. Weber, W. F. Koehl, J. B. Varley, A. Janotti, B. B. Buckley, C. G. Van de Walle, and D. D. Awschalom, *J. Appl. Phys.* **109**, 102417 (2011).
- <sup>10</sup>P. G. Baranov, S. B. Orlinskii, and I. V. Borovykh, *Phys. Rev. B Condens. Matter* **83**, 125203 (2011).
- <sup>11</sup>D. Riedel *et al.*, *Phys. Rev. Lett.* **109**, 226402 (2012).
- <sup>12</sup>C. G. Hemmingsson, N. T. Son, A. Ellison, J. Zhang, and E. Janzén, *Phys. Rev. B* **58**, R10119 (1998).
- <sup>13</sup>C. G. Hemmingsson, N. T. Son, O. Kordina, J. P. Bergman, E. Janzén, J. L. Lindström, S. Savage, and N. Nordell, *J. Appl. Phys.* **81**, 6155 (1997).
- <sup>14</sup>Y. Negoro, T. Kimoto, and H. Matsunami, *Appl. Phys. Lett.* **85**, 1716 (2004).

- <sup>15</sup>I. Pintilie, L. Pintilie, K. Irmscher, and B. Thomas, *Appl. Phys. Lett.* **81**, 4841 (2002).
- <sup>16</sup>J. Zhang, L. Storasta, J. P. Bergman, N. T. Son, and E. Janzén, *J. Appl. Phys.* **93**, 4708 (2003).
- <sup>17</sup>K. Danno, T. Hori, and T. Kimoto, *J. Appl. Phys.* **101**, 053709 (2007).
- <sup>18</sup>L. Storasta, H. Tsuchida, T. Miyazawa, and T. Ohshima, *J. Appl. Phys.* **103**, 013705 (2008).
- <sup>19</sup>T. Kimoto *et al.*, *Appl. Phys. Lett.* **67**, 2833 (1995).
- <sup>20</sup>K. Danno and T. Kimoto, *J. Appl. Phys.* **100**, 113728 (2006).
- <sup>21</sup>T. Hornos, A. Gali, and B. G. Svensson, *Mater. Sci. Forum* **679-680**, 261 (2011).
- <sup>22</sup>K. Szász, V. Ivády, I. A. Abrikosov, E. Janzén, M. Bockstedte, and A. Gali, *Phys. Rev. B* **91**, 121201 (2015).
- <sup>23</sup>J.-I. Iwata, C. Shinez, and A. Oshiyama, *Phys. Rev. B* **93**, 125202 (2016).
- <sup>24</sup>J. Coutinho, V. J. B. Torres, K. Demmouche, and S. Öberg, *Phys. Rev. B* **96**, 174105 (2017).
- <sup>25</sup>T. Kobayashi, K. Harada, Y. Kumagai, F. Oba, and Y.-i. Matsushita, *J. Appl. Phys.* **125**, 125701 (2019).
- <sup>26</sup>M. Bockstedte, A. Mattausch, and O. Pankratov, *Phys. Rev. B* **68**, 205201 (2003).
- <sup>27</sup>A. Zywietz, J. Furthmüller, and F. Bechstedt, *Phys. Rev. B* **62**, 6854 (2000).
- <sup>28</sup>A. Zywietz, J. Furthmüller, and F. Bechstedt, *Phys. Rev. B* **59**, 15166 (1999).
- <sup>29</sup>L. Torpo, M. Marlo, T. E. M. Staab, and R. M. Nieminen, *J. Phys. Condens. Matter* **13**, 6203 (2001).
- <sup>30</sup>J. Wiktor, G. Jomard, and M. Bertolus, *Nucl. Instrum. Methods Phys. Res. Sect. B* **327**, 63 (2014).
- <sup>31</sup>J. Heyd and G. E. Scuseria, *J. Chem. Phys.* **118**, 8207 (2003).
- <sup>32</sup>J. Paier, M. Marsman, K. Hummer, G. Kresse, I. C. Gerber, and J. G. Angyán, *J. Chem. Phys.* **124**, 154709 (2006).
- <sup>33</sup>A. Csóré and Á. Gali, *Mater. Sci. Forum* **897**, 269 (2017).
- <sup>34</sup>G. Kresse and J. Furthmüller, *Phys. Rev. B Condens Matter* **54**, 11169 (1996).
- <sup>35</sup>J. P. Perdew, K. Burke, and M. Ernzerhof, *Phys. Rev. Lett.* **77**, 3865 (1996).
- <sup>36</sup>G. Henkelman, B. P. Uberuaga, and H. Jónsson, *J. Chem. Phys.* **113**, 9901 (2000).
- <sup>37</sup>S.-H. Wei, *Comput. Mater. Sci.* **30**, 337 (2004).
- <sup>38</sup>J. Ma, S.-H. Wei, T. A. Gessert, and K. K. Chin, *Phys. Rev. B* **83**, 245207 (2011).

Supplemental Material for *First-principles Study of Electronic and Diffusion Properties of Intrinsic Defects in 4H-SiC*

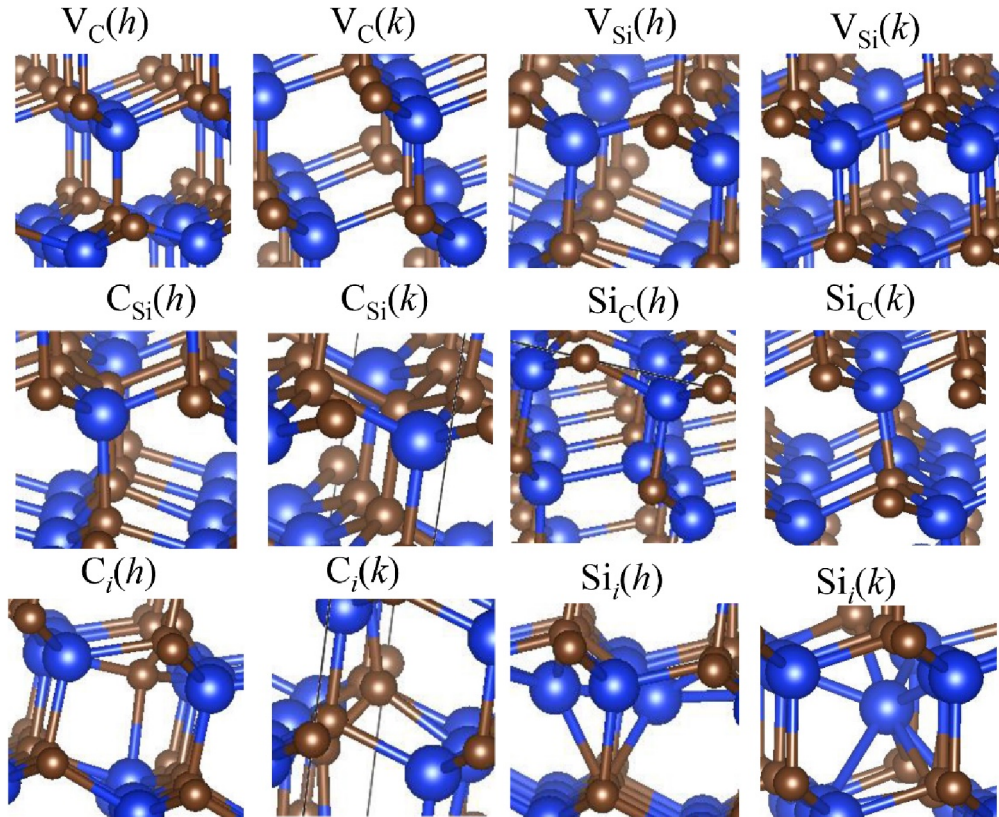


**Fig. S1 Local defect configurations of all the intrinsic defects discussed in the main text.**

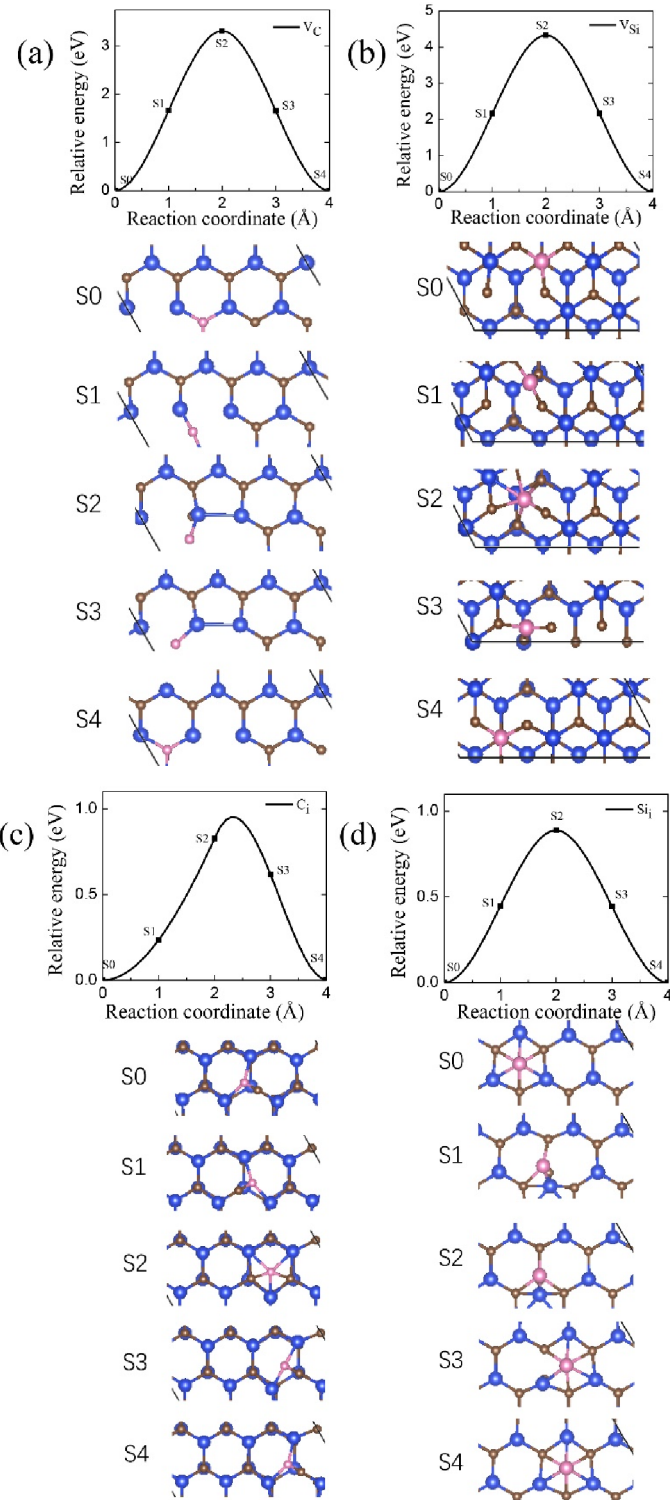


**Fig. S2 Diffusion energy barriers, along with the image structures, along the migration paths for (a)  $V_C$ , (b)  $V_{\text{Si}}$ , (c)  $C_i$  and (d)  $Si_i$  in 4H-SiC.**

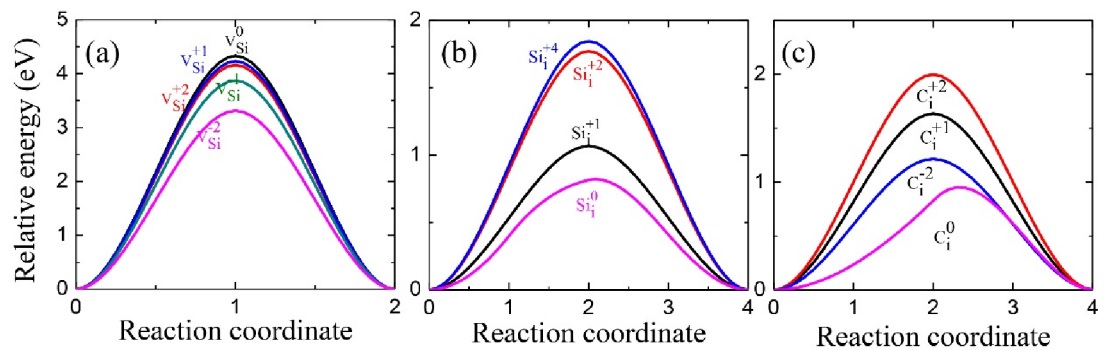


**Fig. S3 Diffusion energy barriers of (a)  $V_{Si}$ , (b)  $C_i$  and (C)  $Si_i$  at different stable charge states.**